coatings

MDPI

Article

Effect of Surface Roughness on Fretting Wear of SLM-Fabricated IN 718 Alloy

Sheng Wang [1,*], Yanping Zeng [2], Wenjuan Wang [1], Xiguo Chen [1] and Qinjiang Fu [1]

[1] Department of Mechanical Engineering, Quzhou College of Technology, Quzhou 324000, China; 155816@qzct.edu.cn (W.W.); xgvip@163.com (X.C.); qj741205704@foxmail.com (Q.F.)
[2] Zhejiang Sunhi-Mach Co., Ltd., Quzhou 324000, China; gang861109@163.com
* Correspondence: wangsheng@qzct.edu.cn

Abstract

To investigate the effect of surface roughness on the fretting wear behavior of the Inconel 718 alloy, specimens fabricated by selective laser melting (SLM) were polished using SiC abrasive papers to obtain different surface roughness levels. Ball-on-flat tangential fretting tests were conducted under a normal load of 50 N, displacement amplitudes of 50 and 100 μm, and a total of 10^4 cycles. The results reveal that all test conditions fall within the gross slip regime (GSR). The coefficient of friction was not significantly affected by surface roughness, while the energy dissipation per cycle exhibited a decreasing trend with decreasing roughness. The high-roughness surface (R_a = 0.80 μm) exhibited severe stress concentration, leading to asperity fracture and fatigue delamination. The medium-roughness specimen (R_a = 0.43 μm) developed a dense third-body layer, showing a synergistic mechanism of abrasive and fatigue wear. The low-roughness specimen (R_a = 0.07 μm) maintained a stable contact interface with sufficient debris evacuation, dominated by adhesive and abrasive wear. At a displacement amplitude of D = 100 μm, the wear depth reached −6 μm, indicating the largest material removal and the most severe damage.

Keywords: Inconel 718; selective laser melting (SLM); surface roughness; fretting wear

1. Introduction

Inconel 718 (IN 718) is a precipitation-hardened nickel-based superalloy that has been extensively employed in critical load-bearing components of aero-engines, gas turbines, and aerospace structures owing to its excellent high-temperature strength, outstanding creep resistance, and superior fatigue performance [1–3]. However, conventional manufacturing routes face inherent limitations in terms of geometric complexity, dimensional accuracy, and design flexibility when fabricating advanced aerospace components. In this context, selective laser melting (SLM) has emerged as a promising additive manufacturing technique for producing IN 718 components, benefiting from its near-net-shape capability, reduced assembly requirements, and high material utilization efficiency [4–6].

In aerospace and other engineering applications, SLM-fabricated IN 718 components are frequently subjected to small-amplitude relative sliding conditions, such as disk–blade dovetail joints, bolted interfaces, and contact assembly regions [7–9]. Under such conditions, the contact interfaces are prone to fretting wear, which is typically characterized by localized damage, wear debris generation, and crack initiation induced by small-amplitude reciprocating motion [10]. It has been widely reported that, owing to the

Check for updates

Academic Editor: Raul Arrabal

Received: 26 December 2025
Revised: 22 January 2026
Accepted: 9 February 2026
Published: 11 February 2026

Copyright: © 2026 by the authors. Licensee MDPI, Basel, Switzerland. This article is an open access article distributed under the terms and conditions of the Creative Commons Attribution (CC BY) license.

high sensitivity of fretting damage to the interfacial contact state, variations in surface roughness can significantly modify the real contact area, local stress distribution, and wear debris behavior; therefore, surface roughness is regarded as one of the key factors governing fretting wear behavior [11]. In fundamental studies on friction and fretting, Ramesh et al. [12] compared the sliding friction behavior of precision-finished surfaces produced by grinding, hard turning, honing, and isotropic polishing, and demonstrated that three-dimensional roughness parameters are strongly correlated with the coefficient of friction, with surface texture orientation playing a critical role in regulating frictional anisotropy. Kubiak et al. [13,14] further indicated that surface roughness not only affects the friction level but also significantly governs the transition from partial slip to gross slip as well as the activation of wear processes: rougher surfaces generally exhibit lower friction coefficients but higher wear rates, whereas smoother surfaces, despite slightly higher friction, tend to delay wear initiation and reduce wear rates. From numerical simulation and operating-condition perspectives, Pereira et al. [15] employed multiscale finite element analysis and found that, under gross sliding conditions, surface roughness markedly alters the contact pressure distribution at the microscale, while its influence on the macroscopic steady-state wear morphology is relatively limited. In lubricated fretting, Lenart et al. [16] further demonstrated that the effect of surface roughness is load-dependent: at lower normal loads, higher roughness is beneficial in reducing friction and wear, whereas at higher loads, an increase in roughness leads to an increase in the friction coefficient. In addition, Varenberg et al. [17] emphasized the critical regulatory role of wear debris in fretting wear, pointing out that surface topography can exert either a promoting or inhibiting effect on wear by influencing debris retention, transport, and third-body effects. Nevertheless, some studies have suggested that, during the steady-state fretting regime or in specific material systems, surface roughness is not the dominant controlling factor [18,19]. In particular, Karagiannidis et al. [20] investigated the friction and wear behavior of additively manufactured IN 718 alloys and found that surface finish mainly influences friction during the running-in stage, while no pronounced differences were observed between as-built and polished specimens under steady-state conditions. Notably, studies specifically addressing fretting wear in SLM-fabricated IN 718 remain scarce, and the fretting wear behavior and associated damage evolution mechanisms under different surface roughness conditions have not yet been systematically clarified.

Based on the above research background, the present study focuses on SLM-fabricated IN 718 alloy and systematically investigates its fretting wear behavior under different surface roughness conditions. Fretting wear experiments were conducted to examine the influence of surface roughness on the evolution of the coefficient of friction, wear morphology, and transitions in wear modes. By correlating the frictional response with detailed wear feature analysis, the role and underlying mechanisms of surface roughness during the fretting wear process are further discussed. This study aims to elucidate the intrinsic relationship between surface roughness and fretting wear behavior of SLM-fabricated IN 718 alloy, thereby providing experimental evidence and theoretical insight for surface state optimization and improved service reliability in aerospace engineering applications.

2. Experiment

2.1. Materials

The raw material used in this study was gas-atomized IN 718 alloy powder produced by AVIC Maite Powder Metallurgy Technology Co., Ltd. in Xuzhou, China. The chemical composition is shown in Table 1, and the particle morphology and size distribution are presented in Figure 1. As shown in the figure, most IN 718 alloy particles exhibit spherical

or near-spherical shapes, with a small number of satellite particles. The particle size ranges from 15 to 53 μm, with a median diameter of 32.5 μm. The samples were fabricated by laser powder bed fusion (LPBF), commercially referred to as selective laser melting (SLM), using an EOS M100 selective laser melting system manufactured in Germany. The build substrate was a 45# steel plate with dimensions of Φ100 mm × 20 mm. Prior to fabrication, the substrate surface was ground to achieve a surface roughness (R_a) below 20 μm, followed by cleaning with alcohol, air-drying, and sealing to prevent oxidation or rusting, which could adversely affect the printing quality. The dimensions of the printed samples were 55 mm × 40 mm × 20 mm. Through repeated printing trials, the optimal process parameters were determined, as listed in Table 2: laser power 100 W, hatch spacing 40 μm, scan speed 1000 mm/s, layer thickness 30 μm, vertical building direction, and an interlayer rotation angle of 67° between adjacent layers. The entire build chamber (including the powder bed and substrate) was heated to 120 °C before SLM forming, with argon used as the protective gas to prevent powder oxidation [21]. The SLM-formed alloy was removed from the substrate using a DK7745 electrical discharge wire-cutting machine and sectioned into alloy samples measuring 40 mm × 20 mm × 5 mm. Based on the application requirements of IN 718 alloy in the aerospace field, the samples were ground and polished using 80#, 800#, and 1500# SiC sandpaper. These surface conditions were made analogous to different post-processing states commonly used in engineering, in order to systematically analyze the influence of surface roughness on fretting wear behavior [22–24]. Subsequently, the samples were ultrasonically cleaned with anhydrous ethanol, dried, and then sealed for storage.

Table 1. Chemical composition of IN 718 alloy powder.

Element	Ni	Cr	Nb	Mo	Ti	Al	Co	Cu	Si	C	Mg	Fe
Content/%	51.08	19.24	5.28	3.13	0.87	0.6	0.19	0.1	0.1	0.05	0.006	Bal.

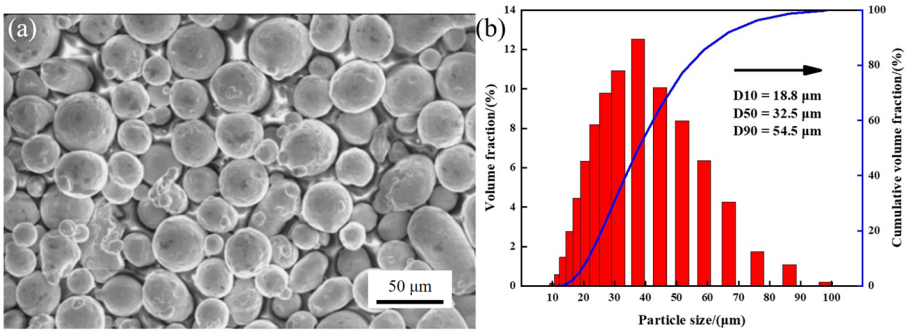

Figure 1. SEM morphology and particle size distribution of IN 718 alloy powder: (**a**) SEM morphology; (**b**) Particle size distribution.

Table 2. SLM process parameters.

Laser Power (W)	Hatch Spacing (μm)	Scan Peed (mm/s)	Layer Thickness (μm)	Scan Strategy
100	40	1000	30	67° interlayer rotation

2.2. Experimental Device

Fretting wear tests were conducted on a self-developed fretting friction and wear testing machine, whose schematic diagram is shown in Figure 2. A ball-on-flat point contact configuration was employed. The tangential displacement was driven by a voice coil motor under PID (Proportional-Integral-Derivative) closed-loop control, generating a

reciprocating tangential displacement of a specific amplitude between the sample and the counter-body ball (Si_3N_4 ball). The normal force was applied using dead weights. The core driving accuracy and sensor measurement accuracy of the testing machine were calibrated by a third-party metrology institution, with their precision ranges meeting the experimental requirements. During the tests, friction force and displacement were acquired and recorded in real time by sensors for plotting the friction force-time curve and F_t-D hysteresis curves.

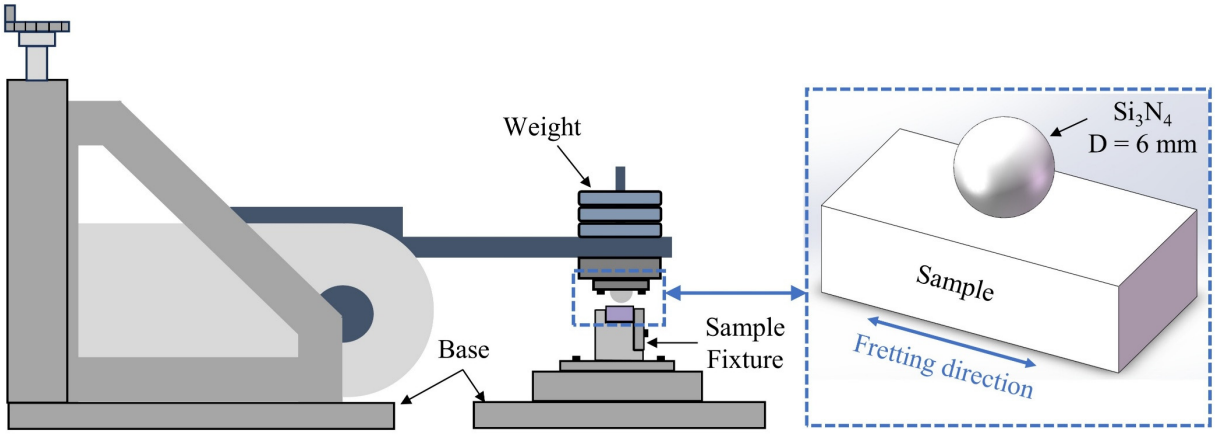

Figure 2. Structural diagram of fretting friction and wear testing machine.

2.3. Analysis Methods

Based on Hertzian contact stress calculations for the tribo-pair, the normal load was set to F_n = 50 N, and the fretting displacement amplitudes were set to D = 50 and 100 μm. Tests were conducted sequentially on the 80#, 800#, and 1500# samples. The number of reciprocating cycles was 1×10^4 for each test, and each parameter set was repeated 3 times. After testing, the morphology of the wear marks was observed using a Sigma 300 field emission scanning electron microscope (SEM) manufactured in Germany. The three-dimensional profiles of the wear scars were characterized using White Light Interferometry (WLI). The damage evolution mechanisms at the fretting interface were analyzed.

3. Results

3.1. Surface Topography Characterization

Figure 3 illustrates the three-dimensional surface morphologies of IN 718 specimens with different pre-treatment conditions prior to fretting tests. Overall, the density of surface asperities shows a pronounced positive correlation with surface roughness. All samples polished with SiC abrasive papers exhibit typical abrasive-induced textures; however, their morphological characteristics evolve markedly with increasing abrasive grit size. The 80# specimen displays pronounced surface undulations with numerous randomly distributed high asperities and deep grooves. As the polishing precision increases to 800#, the amplitude of surface height variation decreases significantly, the transition regions between asperities become smoother, and the grinding-induced textures develop into band-like features aligned with the polishing direction, indicating a distinct surface anisotropy. After 1500# polishing, the rough surface peaks and valleys are almost completely leveled, forming a well-defined parallel texture structure with markedly improved surface flatness and smoothness.

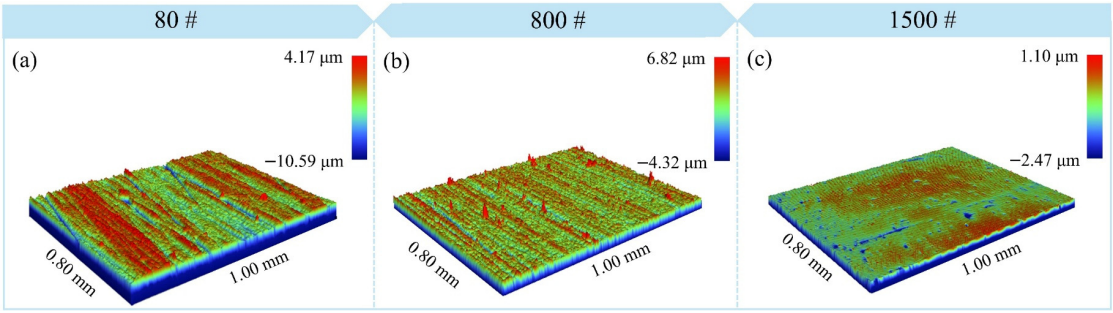

Figure 3. 3D topography images of different samples before wear: (**a**) 80# sample; (**b**) 800# sample; (**c**) 1500# sample.

To further characterize the differences in surface state among the various samples, the cross-sectional profiles and surface roughness of each sample were characterized using a Vision64 white light interferometry system, with the results shown in Figure 4. As observed in Figure 4a, as the sandpaper grit size increased from 80# to 1500#, the peak-to-valley height of the sample surface profiles exhibited a monotonically decreasing trend. The profile curves progressively transitioned from severe fluctuations to gentle and continuous, indicating a significant reduction in the height and distribution variation in surface asperities. This observed trend is consistent with the evolution of the three-dimensional surface topography shown in Figure 3, validating the effective control over surface flatness achieved by the grinding treatment. Furthermore, analysis of the surface roughness parameters (Figure 4b) revealed that after the graded grinding process, the R_a values for the 80#, 800#, and 1500# samples were 0.79 μm, 0.43 μm, and 0.07 μm, respectively. This controlled gradient design in surface roughness provides ideal experimental specimens for the subsequent investigation of the relationship between surface topography characteristics and fretting wear behavior of IN 718.

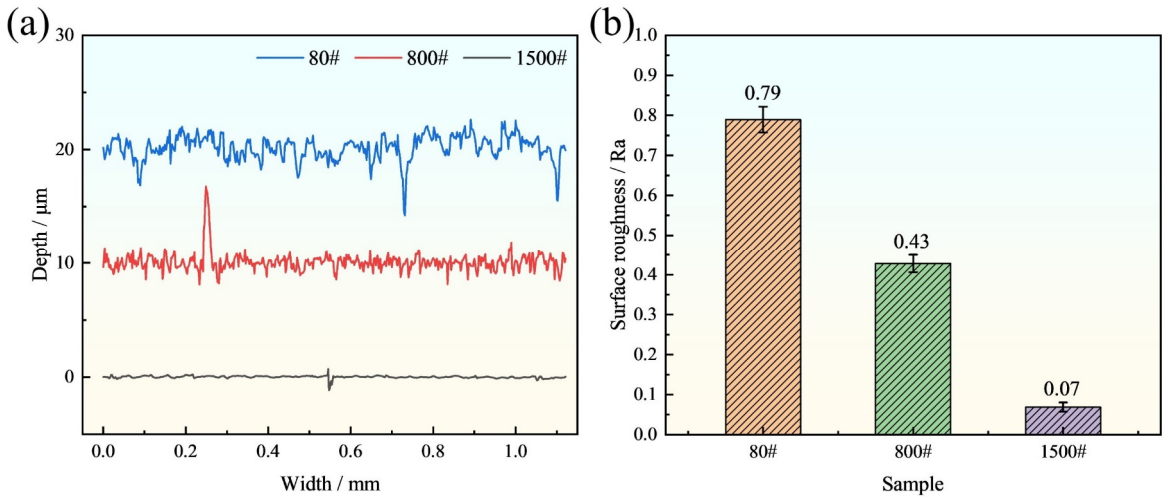

Figure 4. The surface roughness of different samples: (**a**) Representative 2D profiles; (**b**) Surface roughness.

3.2. Fretting Running States

3.2.1. F_t-*D*-*N* Curves

In fretting wear studies, the friction force versus displacement hysteresis loop (F_t-*D*-*N* curve) is the most fundamental and important information reflecting the fretting running regime of the material's contact zone [25,26]. Figure 5 shows the F_t-*D*-*N* curves, illustrating the evolution of the fretting interface with the number of cycles under different displacement amplitudes. The morphology of the F_t-*D*-*N* curves directly

indicates the fretting regime: elliptical or linear-shaped loops characterize the Partial Slip Regime (PSR), parallelogram-shaped loops signify the Gross Slip Regime (GSR), and a transition from elliptical/linear to parallelogram shapes indicates the Mixed Slip Regime (MSR) [27–29]. As shown in Figure 5, when the displacement amplitude was D = 50 μm, the F_t-N curve exhibited a parallelogram shape, indicating that the fretting wear was in the GSR [30]. At displacement amplitudes of D = 50/100 μm, the peak friction force for the 80#, 800#, and 1500# samples demonstrates a trend of first decreasing and then increasing. This phenomenon indicates a significant influence of surface roughness on friction. The 80# sample, with its high roughness and large asperities, exhibits a larger real contact area, resulting in a higher initial peak friction force. However, as the roughness decreases and the asperity size diminishes, the formation of wear debris generates a certain lubricating effect, leading to a slight reduction in the friction force. In contrast, the 1500# sample possesses a smoother surface with smaller, more uniformly distributed asperities, promoting a more homogeneous local stress distribution within the contact zone. Nevertheless, due to its lower surface roughness, the actual contact area is smaller. This reduced contact area results in higher contact pressures, which in turn leads to a slightly higher friction force during the wear process compared to the 800# sample.

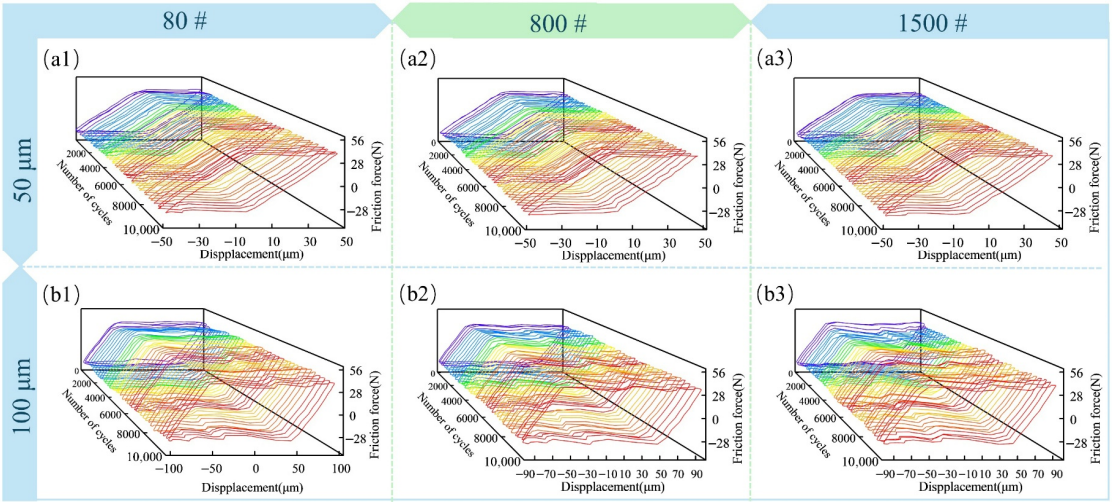

Figure 5. The F_t-D-N curves under different displacement amplitude working conditions: (**a1**–**a3**) represent samples of 80#, 800#, and 1500# at a displacement amplitude of 50 μm; (**b1**–**b3**) represent samples of 80#, 800#, and 1500# at a displacement amplitude of 100 μm.

3.2.2. Energy Dissipation

To further investigate the effect of different roughness levels on fretting wear performance, the area enclosed by the single-cycle F_t-D curve for each condition was calculated, representing the frictional energy dissipated per cycle, as shown in Figure 6a. This enclosed area signifies the degree of damage suffered by the material due to fretting wear [1]. For a given number of cycles, the dissipated energy (E_d) can be calculated using the following formula:

$$E_d = 2\left(\int_{-\delta_0}^{\delta^*} f d\delta - \int_{-\delta_0}^{\delta^*} f d\delta\right) \quad (1)$$

where E_d is the energy dissipated per cycle, f is the friction force, δ_0 is the wear radius (often related to the sticking zone or half the energy-free sliding amplitude, precise definition may vary), $2\delta^*$ is the displacement amplitude, and $d\delta$ represents the incremental change in displacement [31]. By applying this integral to the F_t-D curves obtained from the fretting tests, the energy dissipation values for the samples under different cycles and conditions were determined, as shown in Figure 6b. The results indicate that the dissipated

energy under a displacement amplitude of D = 100 μm is significantly larger compared to D = 50 μm. This is attributed to the increased contact area between the specimen and the counter-body ball at the larger displacement amplitude, which consequently exacerbates fretting wear and material damage [32]. Under both displacement amplitudes, the specimen with a roughness of 0.80 μm (80#) exhibited the highest energy dissipation. Furthermore, a trend of successively decreasing energy dissipation with reducing roughness was observed. This is rationalized by the fact that the 80# sample, with the highest surface roughness and largest real contact area, generated abundant interfacial wear debris, leading to the highest energy dissipation. The 800# sample, with medium roughness, demonstrated moderate debris entrapment and correspondingly lower dissipation. The 1500# sample, possessing the smoothest surface, exhibited stable fretting contact and the lowest frictional work input, resulting in the minimum energy dissipation. However, subsequent wear morphology analysis revealed that energy dissipation cannot directly equate to the extent of material damage. Particularly under high surface finish conditions (low roughness), although the energy dissipation is lower, the wear depth can be more substantial.

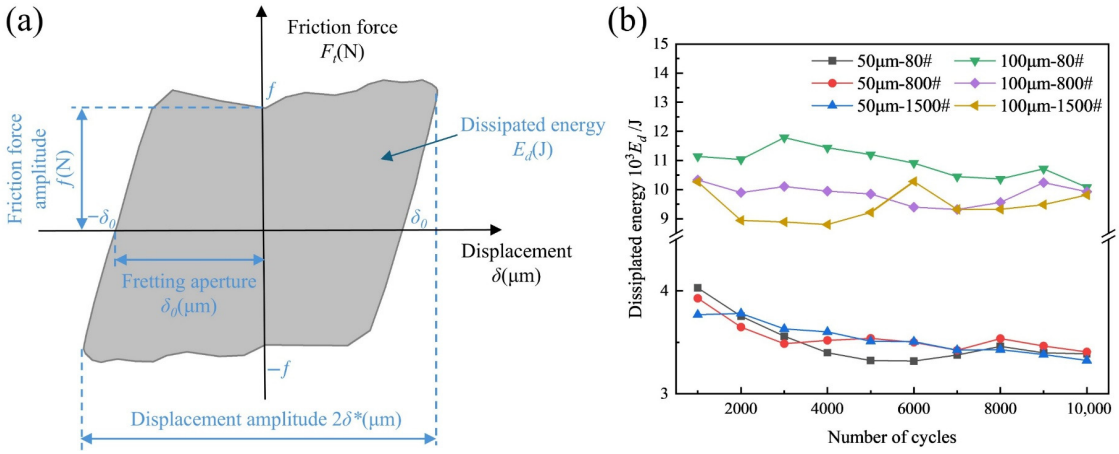

Figure 6. Frictional dissipated energy of SLM formed IN 718 alloys: (**a**) Definition of parameters for calculating dissipated energy from a single-cycle fretting hysteresis loop and (**b**) Dissipated energy statistics for different working conditions.

3.3. Coefficient of Friction

The contact fatigue curve reflects the contact state of the material at the specimen surface during the fretting wear process and plays a significant role in evaluating fretting wear behavior [33]. The friction coefficient curves of the fretting interface under different testing conditions are presented in Figure 7. In tangential fretting wear tests, the temporal evolution of the coefficient of friction (COF) reveals the contact state of the tribo-pair and the behavior of the interfacial third body, as illustrated in Figure 7a. Since the fretting wear consistently occurred in the slip regime, the fretting friction process can be divided into three distinct stages: the running-in stage, the transition stage, and the stable stage [34]. This is attributed to the following mechanistic sequence: during the initial running-in stage, the adsorbed layers and oxide films on the specimen surface are progressively decomposed and spalled, leading to direct contact between the two bodies and a transition to dry friction conditions. Consequently, the COF increases sharply and reaches a maximum. As oxide debris forms and enters the contact interface between the sample and the counter-body, a three-body friction regime is established, leading to a subsequent decrease in the COF. Finally, as the test progresses, a dynamic equilibrium is achieved between the continuous generation and ejection of wear debris, and the COF enters a stable stage [35]. Notably (Figure 7b), at displacement amplitudes D = 50 μm and 100 μm, the average COF for the

80# sample (R_a = 0.80 μm) was 0.73 and 0.76, respectively, higher than that of the 800# sample (R_a = 0.43 μm), which was 0.71 and 0.69. Analysis of surface roughness parameters reveals that the COF exhibits a non-monotonic trend with R_a value, but the variation is relatively small; the average COF values for the 800# and 1500# samples are almost equal.

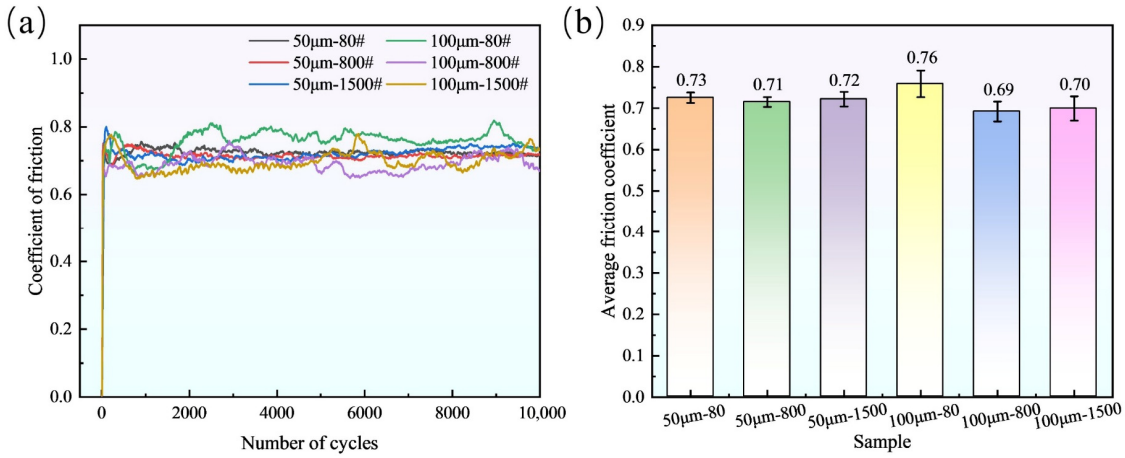

Figure 7. The coefficient of friction curves under different conditions: (**a**) Time-dependent coefficient of friction curves and (**b**) Average coefficient of friction.

3.4. Wear Morphology Analysis

Figure 8 shows the three-dimensional surface morphologies of the fretting wear scars under different test conditions. It can be clearly observed that, at both displacement amplitudes (D = 50 μm and 100 μm), surface roughness has a significant influence on the fretting wear morphology of the SLM-fabricated IN 718 alloy. For the 80# sample with higher surface roughness, the dense distribution of asperities leads to blurred wear boundaries, indicating that local stress concentration intensifies asperity fracture and nonuniform accumulation of wear debris. As surface roughness decreases, the wear scar morphology becomes increasingly regular: the 80# and 800# samples exhibit an elliptical wear scar shape, while the 1500# sample shows an almost circular wear scar. Specifically, at D = 50 μm, the wear scar widths for the 80#, 800#, and 1500# samples are 1.39 mm, 1.34 mm, and 0.54 mm, respectively; at D = 100 μm, the corresponding widths are 1.49 mm, 1.36 mm, and 1.01 mm. The gradual decrease in wear scar width with reduced roughness is attributed to asperity-induced contact behavior. On rougher surfaces, numerous asperities interact intensely with the counterface during sliding, causing severe local stress concentration, larger material removal, and wider wear scars. In contrast, smoother surfaces with fewer asperities provide more uniform contact, more stable frictional behavior, and a milder wear process, leading to narrower wear scars.

Figure 9 presents the two-dimensional wear scar profiles under different test conditions. At a displacement amplitude of D = 50 μm, the wear scar profiles of all samples lie above the unworn reference surface, with the raised height of the 80#, 800#, and 1500# samples ranging approximately from 0 to 5 μm. This phenomenon is attributed to the debris retention mechanism: the small displacement amplitude restricts the expulsion of wear debris, leading to the formation of a compacted debris layer and plastic accumulation at the contact edges, both of which elevate the surface profile. When the displacement amplitude increases to D = 100 μm, only the 1500# sample exhibits a pronounced depression in the wear scar, with a maximum wear depth of approximately −6 μm, while the profiles of the 80# and 800# samples remain above the reference surface. This indicates that a low-roughness surface (such as the 1500# sample), combined with a larger displacement amplitude, facilitates debris evacuation and allows the actual material loss caused by oxidative wear to be clearly

revealed in the wear profile. In contrast, for high- and medium-roughness surfaces, the persistent retention of debris continues to obscure the true wear depth of the substrate.

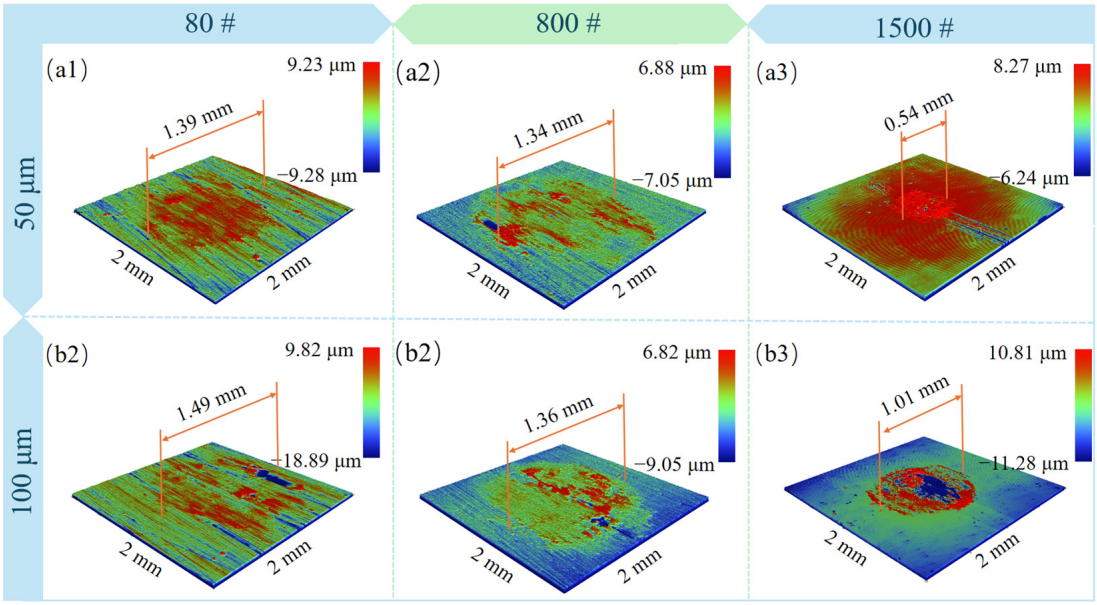

Figure 8. 3D topography images of fretting wear under different working conditions: (**a1**–**a3**) represent samples of 80#, 800#, and 1500# at a displacement amplitude of 50 μm; (**b1**–**b3**) represent samples of 80#, 800#, and 1500# at a displacement amplitude of 100 μm.

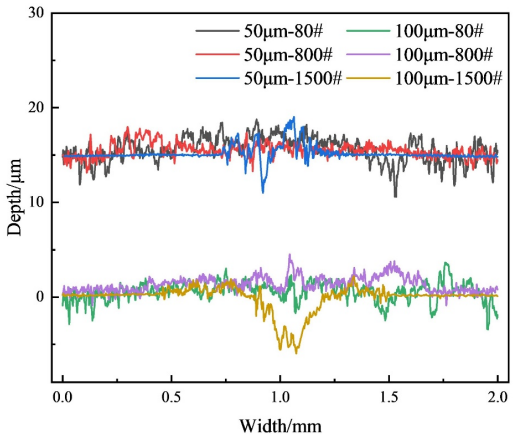

Figure 9. Two-dimensional cross-sectional profiles after wear under different working conditions.

Further analysis in conjunction with the energy dissipation results shows that although the maximum dissipated energy decreases with decreasing surface roughness, the subsequent wear morphology analysis demonstrates that energy dissipation does not directly correlate with the extent of material damage. Under high surface finish conditions (e.g., the 1500# sample), despite lower energy dissipation, the actual contact area between the sample and the counter ball is smaller. Moreover, due to the significant reduction in peak–valley height, the number and volume of surface "valleys" are markedly decreased, leading to a more concentrated real contact region. As a result, the local contact stress level is increased, wear debris is more readily expelled from the contact interface, and a greater wear depth is produced, with a pronounced concave wear profile observed. These results indicate that energy dissipation reflects the energy conversion during the surface friction process, whereas wear depth more directly characterizes the true damage severity of the material. Consequently, the 1500# specimen with lower surface roughness exhibits more severe actual material damage.

Figure 10 shows the SEM morphologies of the worn surfaces of different samples after fretting wear tests. Corroborated by the displacement hysteresis characteristics depicted in Figure 5, all tested conditions were confirmed to operate within the Gross Slip Regime (GSR). At D = 50 μm, SEM analysis indicates that the 80# specimen exhibited significant debris accumulation at the contact edges during friction, with visible crack initiation sites in localized areas. This demonstrates that cyclic shear stress led to the initiation and propagation of surface fatigue cracks, with fatigue wear being its primary wear mechanism [36]. The wear track surface of the 800# specimen was covered with distinct plowing grooves and abrasive cutting marks, accompanied by minor flake-like delamination and granular debris, indicating that its main mechanism was abrasive wear coupled with slight fatigue wear [37]. The wear scar of the 1500# specimen appeared relatively flat with reduced delamination size, showing only fine micro-cracks and localized adhesive pits along with debris generation. Its predominant wear mechanisms were adhesive wear and abrasive wear. At D = 100 μm, the increased displacement facilitated more effective debris ejection. While the 80# and 800# specimens maintained their respective wear mechanisms, the extent of debris retention was notably reduced. In contrast, the 1500# specimen developed pronounced depression within the wear scar, demonstrating more substantial actual material removal from the low-roughness surface under large displacement conditions. This was characterized by an intensified adhesive wear mechanism accompanied by minor abrasive wear, demonstrating the paradoxical outcome where lower energy dissipation under high surface finish conditions corresponds to increased wear depth. Under fretting wear conditions, an excessively low surface roughness does not necessarily result in improved wear resistance. For the 1500# specimen, the lower surface roughness leads to a more concentrated real contact area, thereby increasing the local contact stress. This stress concentration facilitates subsurface damage accumulation and deep material delamination. As a result, although the overall frictional energy dissipation is relatively low, the specimen still exhibits a deeper wear scar. This finding indicates that for SLM-fabricated IN 718 components operating under fretting conditions, an overly fine polishing process may not be the optimal post-processing option. Instead, a surface condition with a certain level of roughness may achieve a more reasonable balance among friction behavior, wear debris accommodation, and wear resistance.

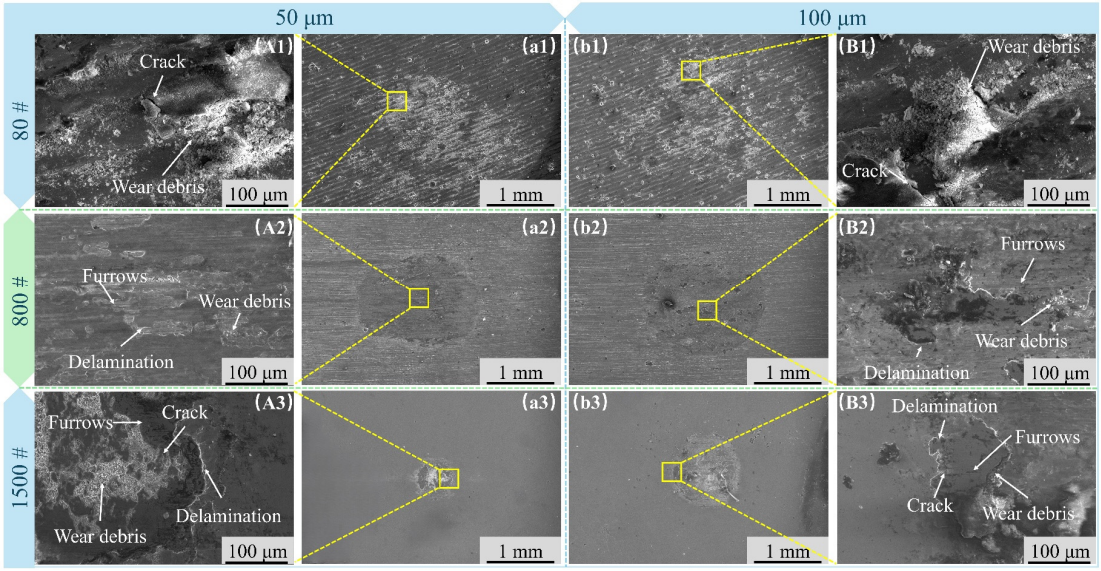

Figure 10. Surface SEM morphology of different samples after fretting wear: (**a1**–**a3**) represent samples of 80#, 800#, and 1500# at a displacement amplitude of 50 μm; (**b1**–**b3**) represent samples of 80#, 800#, and 1500# at a displacement amplitude of 100 μm; (**A1**–**A3**) and (**B1**–**B3**) respectively represent high-magnification enlargements of the yellow-boxed areas.

3.5. Analysis of Damage Evolution

Figure 11 illustrates the evolution process of fretting damage in SLM-fabricated IN 718 alloy with different surface roughness levels. During the initial fretting stage, contact between the Si3N4 ball and the IN 718 surface is primarily governed by localized interactions at asperity junctions. For the highest roughness specimen (80#), the numerous asperity contact points generate severe stress concentration, promoting rapid crack initiation and propagation beneath the asperity tips. As cyclic loading progresses, brittle fracture of asperities occurs, generating substantial wear debris that accumulates at the contact edges to form a non-uniform third-body layer. Concurrent stress accumulation leads to laminated delamination and fatigue crack propagation, establishing a fatigue-dominated wear mechanism. The blurred wear scar boundaries and accumulated debris observed in Figure 10 further validate this mechanism.

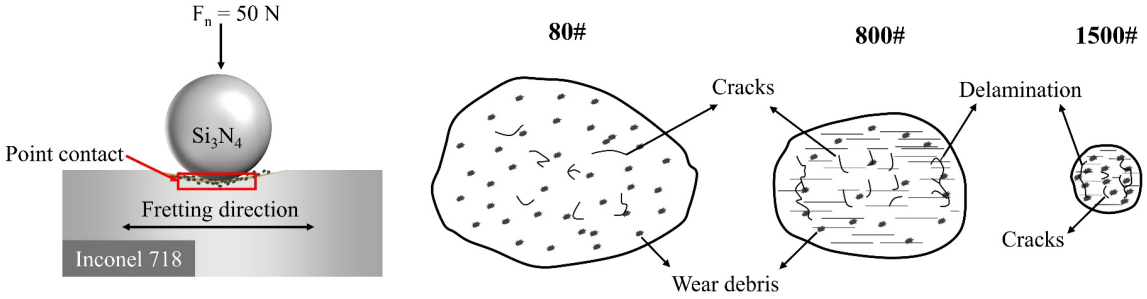

Figure 11. Schematic diagram of damage evolution for IN 718/Si_3N_4 fretting interface under different roughness.

When the roughness decreases to a moderate level (800#), both the quantity and height variation in asperities are significantly reduced. Under these conditions, a uniform and stable third-body layer readily develops, composed of compacted oxide debris and metallic particles. This layer provides certain solid lubricating effects, contributing to friction reduction. The prevailing wear mechanism involves synergistic interaction between abrasive wear and fatigue wear, with the worn surface exhibiting shallow grooves and localized delamination.

At the lowest roughness level (1500#), stress distribution within the contact zone becomes more homogeneous, resulting in stabilized interfacial contact. The wear scar center shows extensive plowing grooves and delamination pits caused by adhesion, indicating combined adhesive wear and abrasive wear mechanisms. Under the displacement amplitude of D = 100 μm, SEM results reveal smooth adhesive pits in the wear scar center (Figure 10), while the wear depth of the 1500# specimen reaches −6 μm in Figure 9, reflecting the maximum actual material removal. These findings demonstrate that while reduced roughness promotes more stable friction behavior, it simultaneously accelerates material removal, ultimately leading to more severe damage.

4. Conclusions

The fretting wear behavior of SLM-fabricated IN 718 samples with different surface roughness levels was systematically investigated. The main conclusions are as follows:

(1) The fretting behavior of all specimens resides within the Gross Slip Regime (GSR). While the coefficient of friction shows no significant correlation with surface roughness, the energy dissipation exhibits a sequential decreasing trend with reduced roughness. However, energy dissipation alone cannot directly reflect the extent of material damage. Particularly under high surface finish conditions, although energy dissipation is lower, the wear depth is more substantial.

(2) Surface roughness significantly influences the wear scar morphology and damage mechanisms of the SLM-fabricated IN 718 alloy. The high-roughness (80#) surface experiences severe stress concentration, leading to prone asperity fracture and fatigue delamination. The medium-roughness (800#) specimen develops a compact third-body layer, demonstrating synergistic characteristics of abrasive wear and fatigue wear. The low-roughness (1500#) specimen maintains stable contact interface conditions with efficient debris ejection, exhibiting adhesive wear and abrasive wear mechanisms that result in the maximum actual material removal and consequently more severe damage.

Author Contributions: Conceptualization, S.W.,Y.Z. and X.C.; methodology, S.W.; software, X.C.; validation, S.W.,W.W., X.C. and Q.F.; formal analysis, S.W.; investigation, S.W.; resources, S.W.; data curation, S.W.; writing—original draft preparation, S.W. and Y.Z.; writing—review and editing, S.W. and W.W.; visualization, W.W., X.C. and Q.F.; supervision, S.W.; project administration, S.W.; funding acquisition, S.W. All authors have read and agreed to the published version of the manuscript.

Funding: This work was supported by the Science and Technology Major Projects of Quzhou, grant number 2025K124, 2025K154.

Institutional Review Board Statement: Not applicable.

Informed Consent Statement: Not applicable.

Data Availability Statement: Data are contained within the article.

Conflicts of Interest: Author Yanping Zeng.is employed by Zhejiang Sunhi-Mach Co., Ltd. The remaining authors declare that the research was conducted in the absence of any commercial or financial relationships that could be construed as a potential conflict of interest.

References

1. Xu, Z.; Lu, H.; Zeng, X.; Wang, X.; Wu, H.; Peng, J.; Zhu, M. A Study on the Fretting Wear Characteristic of Inconcel 718 Alloys Formed by Selective Laser Melting(SLM). *Wear* **2025**, *571*, 205858. [CrossRef]
2. Xu, Z.; Huang, Z.; Zhang, J.; Xu, X.; Li, P.; Su, F.; Zhu, M. Tribological Behaviors and Microstructure Evolution of Inconel 718 Superalloy at Mid-High Temperature. *J. Mater. Res. Technol.* **2021**, *14*, 2174–2184. [CrossRef]
3. Amanov, A. Improvement in Mechanical Properties and Fretting Wear of Inconel 718 Superalloy by Ultrasonic Nanocrystal Surface Modification. *Wear* **2020**, 446–447, 203208. [CrossRef]
4. Trosch, T.; Strößner, J.; Völkl, R.; Glatzel, U. Microstructure and Mechanical Properties of Selective Laser Melted Inconel 718 Compared to Forging and Casting. *Mater. Lett.* **2016**, *164*, 428–431. [CrossRef]
5. Gao, B.; Zhao, H.; Peng, L.; Sun, Z.; Gao, B.; Zhao, H.; Peng, L.; Sun, Z. A Review of Research Progress in Selective Laser Melting (SLM). *Micromachines* **2022**, *14*, 57. [CrossRef]
6. Wang, Q.; Gao, M.; Li, Q.; Liu, C.; Li, L.; Li, X.; Liu, Z. A Review on Energy Consumption and Efficiency of Selective Laser Melting Considering Support: Advances and Prospects. *Int. J. Precis. Eng. Manuf.-Green Tech.* **2024**, *11*, 259–276. [CrossRef]
7. Anandavel, K.; Prakash, R.V. Effect of Three-Dimensional Loading on Macroscopic Fretting Aspects of an Aero-Engine Blade–Disc Dovetail Interface. *Tribol. Int.* **2011**, *44*, 1544–1555. [CrossRef]
8. Lee, B.-W.; Suh, J.; Lee, H.; Kim, T. Investigations on Fretting Fatigue in Aircraft Engine Compressor Blade. *Eng. Fail. Anal.* **2011**, *18*, 1900–1908. [CrossRef]
9. Qu, Z.; Yao, C.; Zhu, H.; Lin, X.; Chen, L.; Zhang, Z.; Fang, J. Research on the Effect of Fretting Wear on the Vibration Characteristics of the Tenon Joint Bladed Disk. *J. Phys. Conf. Ser.* **2024**, *2707*, 012115. [CrossRef]
10. Jiang, C.-P.; Masrurotin; Wibisono, A.T.; Macek, W.; Ramezani, M. Enhancing Internal Cooling Channel Design in Inconel 718 Turbine Blades via Laser Powder Bed Fusion: A Comprehensive Review of Surface Topography Enhancements. *Int. J. Precis. Eng. Manuf.* **2025**, *26*, 487–511. [CrossRef]
11. Strano, G.; Hao, L.; Everson, R.M.; Evans, K.E. Surface Roughness Analysis, Modelling and Prediction in Selective Laser Melting. *J. Mater. Process. Technol.* **2013**, *213*, 589–597. [CrossRef]
12. Singh, R.; Melkote, S.N.; Hashimoto, F. Frictional Response of Precision Finished Surfaces in Pure Sliding. *Wear* **2005**, *258*, 1500–1509. [CrossRef]

13. Kubiak, K.J.; Liskiewicz, T.W.; Mathia, T.G. Surface Morphology in Engineering Applications: Influence of Roughness on Sliding and Wear in Dry Fretting. *Tribol. Int.* **2011**, *44*, 1427–1432. [CrossRef]
14. Kubiak, K.J.; Mathia, T.G.; Fouvry, S. Interface Roughness Effect on Friction Map under Fretting Contact Conditions. *Tribol. Int.* **2010**, *43*, 1500–1507. [CrossRef]
15. Pereira, K.; Yue, T.; Abdel Wahab, M. Multiscale Analysis of the Effect of Roughness on Fretting Wear. *Tribol. Int.* **2017**, *110*, 222–231. [CrossRef]
16. Lenart, A.; Pawlus, P.; Dzierwa, A.; Wos, S.; Reizer, R.; Lenart, A.; Pawlus, P.; Dzierwa, A.; Wos, S.; Reizer, R. The Effect of Surface Texture on Lubricated Fretting. *Materials* **2020**, *13*, 4886. [CrossRef]
17. Varenberg, M.; Halperin, G.; Etsion, I. Different Aspects of the Role of Wear Debris in Fretting Wear. *Wear* **2002**, *252*, 902–910. [CrossRef]
18. Yoon, Y.; Etsion, I.; Talke, F.E. The Evolution of Fretting Wear in a Micro-Spherical Contact. *Wear* **2011**, *270*, 567–575. [CrossRef]
19. Raeymaekers, B.; Talke, F.E. The Effect of Laser Polishing on Fretting Wear between a Hemisphere and a Flat Plate. *Wear* **2010**, *269*, 416–423. [CrossRef]
20. Karagiannidis, I.; Tzanis, A.; Drees, D.; Lopes, L.; Chondrakis, G.; Dardavila, M.M.; Georgiou, E.; Koutsomichalis, A.; Karagiannidis, I.; Tzanis, A.; et al. Friction and Wear Behavior of 3D-Printed Inconel 718 Alloy under Dry Sliding Conditions. *Coatings* **2024**, *14*, 1029. [CrossRef]
21. Bean, G.E.; Witkin, D.B.; McLouth, T.D.; Zaldivar, R.J. Process Gas Influence on Microstructure and Mechanical Behavior of Inconel 718 Fabricated via Selective Laser Melting. *Prog. Addit. Manuf.* **2020**, *5*, 405–417. [CrossRef]
22. McRoskey, J.; Busse, M. Effects of Surface Finish on High Cycle Fatigue of Inconel 718. *Mater. Eng*. **2020**. Available online: https://digitalcommons.calpoly.edu/matesp/229 (accessed on 8 February 2026).
23. Szablewski, P. Evaluation of the Topography and Load Capacity of Cylindrical Surfaces Shaped in the Process of Finish Turning of the Inconel 718 Alloy. *Measurement* **2023**, *223*, 113749. [CrossRef]
24. Wang, L.; Sun, Y.; Xiao, Z.; Yao, L.; Guo, J.; Kang, S.; Mao, W.; Zuo, D. Experimental Investigation on Magnetic Abrasive Finishing for Internal Surfaces of Waveguides Produced by Selective Laser Melting. *Materials* **2024**, *17*, 1523. [CrossRef]
25. Nie, H.; Ren, Y.; Li, Y.; He, J.; Huang, G.; Peng, J.; Zhu, M. Composite Fretting Wear Characteristics of EA4T Axle Steel Under Radial and Tangential Loads. *Tribology* **2024**, *44*, 1505–1515. [CrossRef]
26. Hu, J.; Xia, D.; Cai, Y.; Wang, S.; Sun, Z.; Cui, Y.; Jiang, K.; Li, T.; Zhang, H.; Chen, T.; et al. Effect of Normal Load on Fretting Wear Behaviour of GCr15 Bearing Steel. *J. Phys. Conf. Ser.* **2025**, *2956*, 012010. [CrossRef]
27. Hu, Y.; Zhang, X.; Jia, H.; Yang, X.; Chai, L.; Wang, S. High-Temperature Fretting Wear Behavior of IN738LC Alloy Formed by Laser Powder Bed Fusion. *Tribol. Int.* **2024**, *199*, 110017. [CrossRef]
28. Wei, S.; Kaimin, L.; Wanjia, L.; Wanwu, D. Effect of Fretting Wear on TC4 Alloy Prepared by Laser Shock Peening at High Temperature. *Surf. Eng.* **2024**, *40*, 112–124. [CrossRef]
29. Ning, C.; Li, K.; Tang, G.; Xie, Y.; Shang, L.; Zhang, G.; Cai, Z. Fretting Wear Performance of CrN Coating after Laser Shock Peening. *Chin. J. Mech. Eng.* **2025**, *38*, 96. [CrossRef]
30. Zhu, M.H.; Zhou, Z.R. On the Mechanisms of Various Fretting Wear Modes. *Tribol. Int.* **2011**, *44*, 1378–1388. [CrossRef]
31. Xu, Z.; Li, D.; Lu, Z.; Lv, X.; Liu, Y.; Peng, J.; Zhu, M. Study on the Damage Evolution of Fretting Wear in an Inconel 718 Laser Cladding Alloy Layer at Different Temperatures. *Tribol. Int.* **2023**, *179*, 108092. [CrossRef]
32. Esteves, M.; Ramalho, A.; Ramos, F. Electrical Performance of Textured Stainless Steel under Fretting. *Tribol. Int.* **2017**, *110*, 41–51. [CrossRef]
33. Imran, M.; Wang, D.; Zhou, Y.; Wang, L.; Abdel Wahab, M. Simulation of Fretting Wear in Steel Wires under Variable Coefficient of Friction and Variable Wear Coefficient. *Simul. Model. Pract. Theory* **2024**, *134*, 102959. [CrossRef]
34. Yue, T.; Wahab, M.A. A Review on Fretting Wear Mechanisms, Models and Numerical Analyses. *Comput. Mater. Contin.* **2019**, *59*, 405. [CrossRef]
35. Yao, J.; Lv, L.; He, Y.; Wang, D. Size Effect of (Al_2O_3–Y_2O_3)/YSZ Micro-Laminated Coating on High-Temperature Oxidation Resistance. *Appl. Surf. Sci.* **2013**, *279*, 85–91. [CrossRef]
36. Yuan, X.; Li, G.; Zhang, X.; Pu, J.; Ren, P. An Experimental Investigation on Fretting Wear Behavior of Copper–Magnesium Alloy. *Wear* **2020**, 462–463, 203497. [CrossRef]
37. Arnaud, P.; Fouvry, S.; Garcin, S. A Numerical Simulation of Fretting Wear Profile Taking Account of the Evolution of Third Body Layer. *Wear* **2017**, *376–377*, 1475–1488. [CrossRef]

Disclaimer/Publisher's Note: The statements, opinions and data contained in all publications are solely those of the individual author(s) and contributor(s) and not of MDPI and/or the editor(s). MDPI and/or the editor(s) disclaim responsibility for any injury to people or property resulting from any ideas, methods, instructions or products referred to in the content.